2-18-2008

Relativistic Particle-In-Cell Simulation of Prompt and Early Afterglows from GRBs

K.-I. Nishikawa
National Space Science and Technology Center & Center for Space Plasma and Aeronomic Research, University of Alabama in Huntsville

P. Hardee
Department of Physics and Astronomy, The University of Alabama

Y. Mizuno
National Space Science and Technology Center & NASA Postdoctoral Program Fellow/ NASA Marshall Space Flight Center

M. Medvedev
Department of Physicsa nd Astronomy, University of Kansas

B. Zhang
Department of Physics, University of Nevada

See next page for additional authors

Recommended Citation

Please use publisher's recommended citation.

Authors

K.-I. Nishikawa, P. Hardee, Y. Mizuno, M. Medvedev, B. Zhang, Dieter H. Hartmann, and G. J. Fishman

Relativistic Particle-In-Cell Simulation Studies of Prompt and Early Afterglows from GRBs

K.-I. Nishikawa[1,2], P. Hardee[3], Y. Mizuno[1,8], M. Medvedev[4],
B. Zhang[5], D. H. Hartmann[6], and G. J. Fishman[7]

ABSTRACT

Nonthermal radiation observed from astrophysical systems containing relativistic jets and shocks, e.g., gamma-ray bursts (GRBs), active galactic nuclei (AGNs), and microquasars commonly exhibit power-law emission spectra. Recent PIC simulations of relativistic electron-ion (or electron-positron) jets injected into a stationary medium show that particle acceleration occurs within the downstream jet. In collisionless, relativistic shocks, particle (electron, positron, and ion) acceleration is due to plasma waves and their associated instabilities (e.g., the Weibel (filamentation) instability) created in the shock region. The simulations show that the Weibel instability is responsible for generating and amplifying highly non-uniform, small-scale magnetic fields. These fields contribute to the electron's transverse deflection behind the jet head. The resulting "jitter" radiation from deflected electrons has different properties compared to synchrotron radiation, which assumes a uniform magnetic field. Jitter radiation may be important for understanding the complex time evolution and/or spectra in gamma-ray bursts, relativistic jets in general, and supernova remnants.

[1]National Space Science and Technology Center, 320 Sparkman Drive, VP 62, Huntsville, AL 35805, USA; ken-ichi.nishikawa-1@nasa.gov

[2]Center for Space Plasma and Aeronomic Research, University of Alabama in Huntsville, Huntsville, AL 35899, USA

[3]Department of Physics and Astronomy, The University of Alabama, Tuscaloosa, AL 35487, USA

[4]Department of Physics and Astronomy, University of Kansas, KS 66045, USA

[5]Department of Physics, University of Nevada, Las Vegas, NV 89154, USA

[6]Clemson University, Clemson, SC 29634-0978, USA

[7]NASA Marshall Space Flight Center, NSSTC, VP62, 320 Sparkman Drive, Huntsville, AL 35805, USA

[8]NASA Postdoctoral Program Fellow/ NASA Marshall Space Flight Center

1. Inroduction

Shocks are believed to be responsible for prompt emission from gamma-ray bursts (GRBs) and their afterglows, for variable emission from blazars, and for particle acceleration processes in jets from active galactic nuclei (AGN) and supernova remnants (SNRs). The predominant contribution to the observed emission spectra is often assumed to be synchrotron- and inverse Compton radiation from these accelerated particles (e.g., Piran 1999, 2000, 2005a; Zhang & Meszaros 2004; Meszaros 2002, 2006; Lyutikov 2006; Zhang 2007). It is assumed that turbulent magnetic fields in the shock region lead to Fermi acceleration, producing higher energy particles (e.g., Fermi 1949; Blandford & Eichler 1987). To make progress in understanding emission from these object classes, it is essential to place modeling efforts on a firm physical basis. This requires studies of the microphysics of the shock process in a self-consistent manner (Piran 2005b; Waxman 2006).

1.1. Fermi Acceleration in Test-Particle Simulations with Turbulent Fields

Diffusive shock (Fermi) acceleration schemes that have been applied to non-relativistic shocks have also been applied to particle acceleration in relativistic shocks (Kirk & Schneider 1987; Heavens & Drury 1988; Bednarz & Ostrowski 1998; Gallant & Achterberg 1999; Kirk et al. 2000; Ellison 2001; Achterberg et al. 2001; Ellison & Double 2002; Vieti 2003; Vladimirov, Ellison & Bykov 2006; Niemiec & Ostrowski 2006; Niemiec, Ostrowski, & Pohl 2006). Such acceleration models explicitly, or implicitly, require turbulent conditions downstream from the shock front and assume a pitch angle diffusion model for particle transport near the shock. Particle energies build up through a cumulative process of particle motion across the shock front (e.g., Gallant 2002; Niemiec & Ostrowski 2004). However, highly efficient acceleration processes required by some observations, e.g., the variable flux of TeV gamma-rays from Mrk 421 and Mrk 501, are not easy to reconcile with the diffusive shock acceleration paradigm. For example, Bednarek, Kirk, & Mastichiadis (1996) proposed acceleration by an electric field to provide a sufficiently fast acceleration process and to allow for the escape of TeV photons.

There are considerable theoretical problems with the application of the pitch angle diffusion model to particle transport near relativistic shocks (Ostrowski & Bednarz 2002). Diffusive shock acceleration (DSA) relies on repeated scattering of charged particles by magnetic irregularities (Alfvén waves) to confine the particles near the shocks. However, in relativistic shocks anisotropies in the angular distribution of the accelerated particles are large, and the diffusion approximation for spatial transport breaks down (Achterberg et al. 2001). Despite decades of research, this mechanism is still not understood from first prin-

ciples (Waxman 2006). Particle scattering in collisionless shocks is due to electromagnetic waves. No present analysis self-consistently calculates the generation of these waves, scattering of particles, and their acceleration. Most studies consider, instead, the evolution of the particle distribution adopting some *Ansatz* for the particle scattering mechanism (e.g. diffusion in pitch angle), and the "test particle" approximation, where modifications of shock properties due to a population of high energy particles is neglected (see, however, Ellison & Double 2002; Vladimirov, Ellison & Bykov 2006; Ellison & Bykov 2008). Furthermore, the electron spectral index p is calculated, in both non-relativistic and relativistic cases, with a phenomenological description of electron scattering based on energy equipartition (ϵ_B and ϵ_e) and, therefore, does not provide a complete, self-consistent description of the process (Piran 2005a,b). In particular, these calculations do not allow one to determine the fraction of energy carried by electrons (Waxman 2003; Eichler & Waxman 2005).

1.2. Simulation of Particle Acceleration in Relativistic Collisionless Shocks and Microscopic Processes

The problems mentioned in the previous section can be overcome by detailed, microscopic analyses of energy transfer in collisionless relativistic outflows (Waxman 2006). Most astrophysical shocks are collisionless, with energy dissipation dominated by wave-particle interactions rather than particle-particle collisions (Piran 2005a; Waxman 2006). In particular, proper study of such relativistic collisionless shocks in GRB- and AGN jets requires simulating the microphysics where plasma waves and their associated instabilities (e.g., the Weibel instability, more precisely, mixed mode two-stream filamentation instability) simultaneously lead to particle (electron, positron, and ion) acceleration and magnetic field generation (Weibel 1959; Medvedev & Loeb 1999; Dieckmann et al. 2006, references therein).

Three-dimensional relativistic particle-in-cell (RPIC) simulations have been used to study the microphysical processes in relativistic shocks. Such PIC simulations show that rapid acceleration takes place in situ in the downstream jet, rather than by scattering of particles back and forth across the shock as in the case of classical Fermi acceleration (Silva et al. 2003; Frederiksen et al. 2003, 2004; Hededal et al. 2004; Hededal & Nishikawa 2005; Medvedev et al. 2005; Nishikawa et al. 2003, 2005a,b, 2006a,b; Chang, Spitkovsky & Arons 2008; Spitkovsky 2005, 2008). Three independent simulation studies confirm that relativistic counter-streaming jets do excite the Weibel instability (Weibel 1959), which generates current filaments and associated magnetic fields (Medvedev & Loeb 1999; Brainerd 2000; Pruet et al. 2001; Gruzinov 2001; Milosavljevic, Nakar, & Spitkovsky 2006; Milosavljevic & Nakar, 2006a,b), and accelerates electrons (Silva et al. 2003; Frederiksen et al. 2003, 2004;

Hededal et al. 2004; Hededal & Nishikawa 2005).

1.3. RPIC Simulations of Particle Acceleration and Electromagnetic Field Generation by the Weibel Instability

The code used in this study is a modified version of the TRISTAN code, a relativistic particle-in-cell (RPIC) code (Buneman 1993). Descriptions of PIC codes can be found in Dawson (1983), Birdsall & Langdon (2005), and Hickory & Eastwood (1988). The RPIC code has been parallelized using OpenMP on the Columbia computer system at the NASA Advanced Supercomputing (NAS) facility and the most recent simulations have been performed using the new parallelized version (Ramirez-Ruiz, Nishikawa & Hededal 2007). The code has also been parallelized with MPI, and new results are reported in Niemiec, Pohl, Stroman & Nishikawa (2008).

The spatial development of a relativistic collisionless shock involving a moving jet front was investigated in our previous work (Nishikawa et al. 2003, 2005a,b, 2006a,b; Hededal & Nishikawa 2005). In general, we confirmn the results found in counter-streaming simulations (Silva et al. 2003; Jaroschek, Lesch, & Treumann 2005). Recently, to simulate shock formation, Spitkovsky (2008) reflects a relativistically moving cold electron-ion stream from a conducting wall. This is similar to colliding two streams of identical plasmas head-on but saves one-half of the computational effort (Chang, Spitkovsky, & Arons 2008). By injecting particle jets into the ISM from one side (left in our simulations) of a fixed simulation box, we can study variations in the density of the jet and the ambient medium, the density structure, the magnetic field strength and direction, and the Lorentz factor, in order to investigate forward and reverse shock development with different properties of the fireball ejecta (e.g., Kobayashi et al.2007). In this way we can investigate a relativistically moving system of precursors, shocks, and contact discontinuities that form in collisions of jets with stationary plasmas, with emphasis on radiation signatures from the growing instability (e.g., Hoshino 2008; Dieckmann, Shukla, & Drury 2008). The importance of this kind of simulation, with an injection scheme without reflection off a conducting wall, is described in the review paper by Waxman (2006). We have followed this approach to perform a set of numerical experiments to study the development of relativistic collisionless shocks in the context of GRB physics. Our simulations examine realistic spatial evolution of the resultant collisionless shock, including motion of the transition region (the contact discontinuity).

2. Monoenergetic Pair Jet Injected into Electron-Ion Plasmas

In this section we present a simulation study demonstrating how the Weibel instability grows, generates highly structured magnetic fields, and accelerates particles (Ramirez-Ruiz, Nishikawa, & Hededal 2007). In particle simulations of relativistic electron-positron jets propagating through an unmagnetized electron-positron ambient plasmas, the Weibel instability is excited in the downstream region behind the jet head and dominates other possible two-stream instabilities (Nishikawa et al. 2003, 2005a,b, 2006a,b; Hededal & Nishikawa 2005). This predicted result (Brainerd 2000) for relativistic collisionless shocks is different from non-relativistic collisionless shocks where other two-stream instabilities may grow faster than the Weibel instability (Medvedev, Silva, & Kamionkowski 2006).

Simulations were performed using an $85 \times 85 \times 640$ grid with a total of 380 million particles (27 particles/cell/species for the ambient plasma) and an electron skin depth, $\lambda_{\mathrm{ce}} = c/\omega_{\mathrm{pe}} = 9.6\Delta$ (Δ is the grid scale), sufficient to study nonlinear spatial development (Nishikawa et al. 2005a, 2006a). The time step is $t = 0.013/\omega_{\mathrm{pe}}$, where $\omega_{\mathrm{pe}} = (e^2 n_{\mathrm{e}}/m_{\mathrm{e}})^{1/2}$ is the electron plasma frequency ($n_{\mathrm{e}} = n_{\mathrm{b}}$, where n_{b} is the ambient "background" plasma density). The simulations described below were performed by the newly parallelized OpenMP code on Columbia at NASA Advanced Supercomputing (NAS).
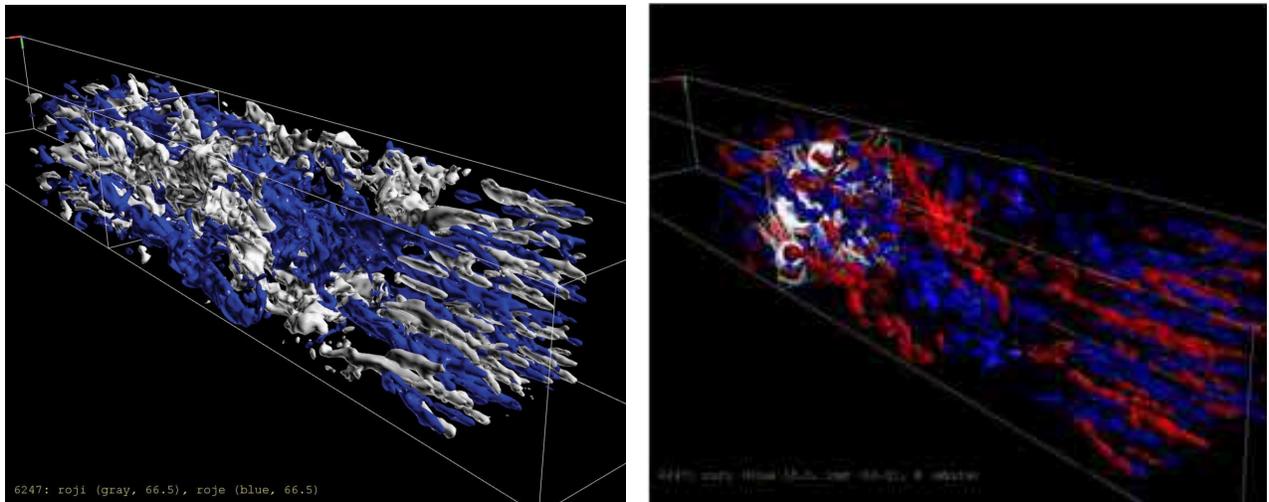

6247: roji (gray, 66.5), roje (blue, 66.5)

Fig. 1.— Snapshots viewed from the front of the jet at $t = 59.8/\omega_{\mathrm{pe}}$, left panel: the isosurface of jet electron (blue) and positron (gray) density, and right panel: the isosurface of the Z-component of the current density (J_{z} :blue and $-J_{\mathrm{z}}$: red) with the magnetic field lines (white) in the linear stage for the case of the mono-energetic jet.

We have simulated four different initial pair jet distributions. Here we present one case, in which a mono-energetic jet ($\gamma V_{\|} = 12.57c$) is injected into an electron-ion ambient plasma,

similar to published simulations (Nishikawa et al. 2005a, 2006a; Ramirez-Ruiz, Nishikawa, & Hededal 2007; Nishikawa et al. 2008). For all cases the jet particles are very cold ($0.01c$ in the rest frame). The mass ratio of electrons to ions in the ambient plasma is $m_i/m_e = 20$. The electron thermal velocity in the ambient plasma is $v_{th,e} = 0.1c$, where c is the speed of light. The ion thermal velocity in the ambient plasma is $v_{th,i} = 0.022c$.

The electron density and currents have a complicated three-dimensional structure due to the excitation of the filamentation instability (Ramirez-Ruiz, Nishikawa, & Hededal 2007). Current filaments (J_z) and their associated magnetic fields (white curves) produced by the filamentation (Weibel) instability form the dominant structures in the relativistic collisionless shock shown in Figure 1. In the linear stage, the transverse size of these structures is nearly equal to the electron skin depth but the longitudinal size (along the jet direction as shown on the left side of the left panel) is much larger. Growing smaller current filaments that appear first in the linear stage far behind the jet front, eventually merge into larger filaments during the nonlinear stage behind the jet front.
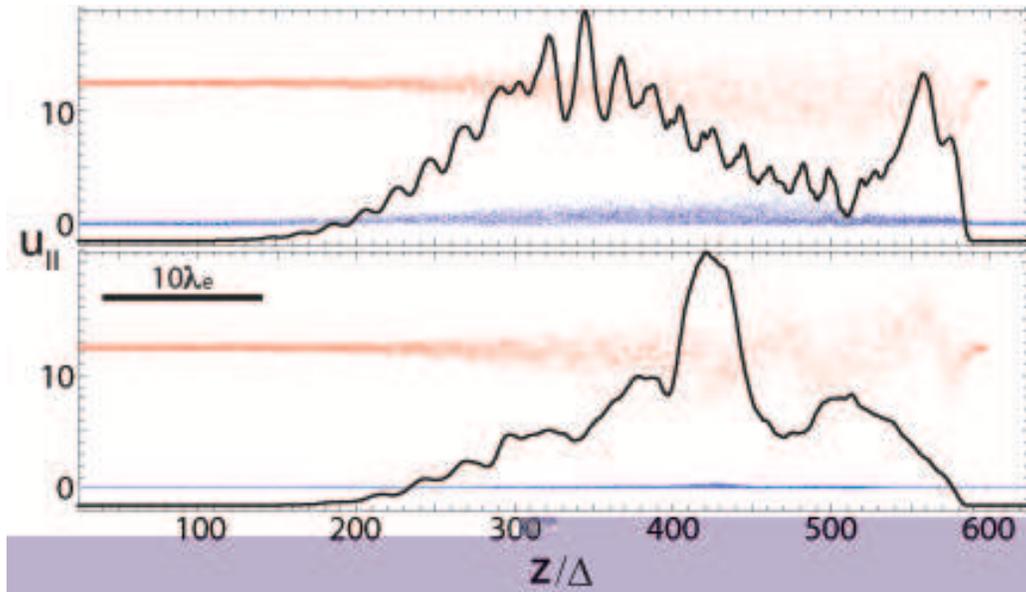

Fig. 2.— Longitudinal heating and acceleration, illustrated by changes in $u_{||}$ for both injected electrons (red) and ambient plasma (blue). The bottom (top) panels are for a simulation in which the ambient medium is composed of electrons and ions ($e^{\pm}$ pairs). Also shown are the average transverse magnetic field amplitude (in arbitrary units) in the $X - Y$ plane as a function of Z/Δ (solid curves).

Encountering the medium at rest, the incoming $e^{\pm}$ pairs are rapidly deflected by field fluctuations. The initial perturbations become non-linear as the deflected $e^{\pm}$ pairs collect into current channels. The resultant toroidal magnetic fields cause mutual attraction between

currents, forcing like currents to approach each other and merge. As a result, the magnetic field grows in strength. This continues until the fields grow strong enough to deflect the much heavier ions (Frederiksen et al. 2004). As illustrated in Fig. 2, the ions stay clearly separated in phase space and are only slowly heated. In the presence of ions, the magnetic field saturates at a higher level, by a factor of $(m_i/m_e)^{1/2} = \sqrt{20} \sim 4.5$, albeit on a longer timescale. The differences are due to the massive ion bulk momentum constituting a dominant energy reservoir available for particle heating (Ramirez-Ruiz, Nishikawa & Hededal 2007). We also found that the broadband (not monoenergetic) jet sustains the stronger magnetic field over a larger region (see Fig. 8 in Ramirez-Ruiz, Nishikawa & Hededal (2007)).

3. Radiation models

3.1. The Standard Synchrotron Radiation Model

Synchrotron emission is widely assumed to be the most important radiation mechanism in the external shock thought to be responsible for the observed broad-band afterglows from GRBs (e.g., Zhang & Meszaros 2004; Piran 2005a; Zhang 2007, Nakar 2007). Associated with this picture are three parameterizations that are adopted in almost all current GRB afterglow models. First, electrons are assumed to be "Fermi"-accelerated at the relativistic shocks and to obtain a power-law distribution in energy, $N(E_e)dE_e \propto E^{-p}dE_e$, with p $\sim$ 2. This is consistent with numerical simulations of shock acceleration (Achterberg et al. 2001; Ellisson & Double 2002; Lemoire & Pelletier 2003).

Second, the strength and geometry of the magnetic fields in the shocked region is unknown, but its energy density $(B^2/8\pi)$ is assumed to be a fraction ϵ_B of the internal energy. The values of "micro-physics" parameters, such as $d\log n_e/d\log\varepsilon = p$ (the energy distribution of the electrons), and the fraction of the energy, ϵ_e, carried by electrons, are usually obtained by fitting afterglow data (e.g., Panaitescu & Kumar 2001; Yost et al. 2003), but are only phenomenological and not based on a full understanding of the underlying microphysics (Waxman 2006).

The typical observed emission frequency from an electron with (comoving) energy $\gamma_e m_e c^2$ in a frame with a bulk Lorentz factor Γ is $\nu = \Gamma\gamma_e^2(eB/2\pi m_e c)$. Three critical frequencies are defined by three characteristic electron energies. These are ν_m (the injection frequency), ν_c (the cooling frequency), and ν_M (the maximum synchrotron frequency). In the afterglow problem, there is one more frequency, ν_a, which is defined by synchrotron self-absorption at lower frequencies (Meszaros, Rees, & Wijers 1998; Sari, Piran, & Narayan 1998; Nakar 2007; Zhang 2007).

The agreement between the dynamics predicted by the blast wave model and the direct measurements of the fireball size strongly argue for the validity of this model's dynamics (e.g., Zhang 2007; Nakar 2007). The shock wave is most likely collisionless, i.e., mediated by plasma instabilities (Waxman 2006), and these electromagnetic instabilities are expected to generate magnetic fields. Afterglow radiation was therefore predicted to result from synchrotron emission of shock accelerated electrons (Meszaros & Rees 1997). The observed afterglow spectra are indeed remarkably consistent with synchrotron emission of electrons accelerated to a power-law energy distribution, thus providing support to the validity of this "standard afterglow model" (Piran 1999, 2000, 2005a; Zhang & Meszaros 2004; Meszaros 2002, 2006; Zhang 2007; Nakar 2007).

In order to determine the luminosity and spectral energy density (SED) of synchrotron radiation, the strength of the field (ϵ_B) and the energy distribution of the electrons (p) must be determined. Due to the lack of a first principles theory of collisionless shocks, a purely phenomenological approach to modeling afterglow radiation is applied, but one must recognize that emission is then calculated without a full understanding of the processes responsible for particle acceleration and magnetic field generation (Waxman 2006). Despite these shortcomings, it is general practise to simply assume that a certain fraction ϵ_B of the post-shock thermal energy density is carried by the magnetic field, that a fraction ϵ_e is carried by electrons, and that the energy distribution of the electrons is a power-law, $d \log n_e / d \log \varepsilon = p$ (above some minimum energy E_m which is determined by ϵ_e, ϵ_B and p). In this approach, ϵ_B, ϵ_e, and p are treated as free parameters, to be determined by observations. It is important to clarify that the constraints implied on these parameters by the observations are independent of any assumptions regarding the nature of the afterglow shock and the processes responsible for particle acceleration or magnetic field generation. Any model proposed for the actual shock micro-physics must be consistent with these phenomenological constraints.

3.2. "Jitter" Radiation from Accelerated Particles in Turbulent Electromagnetic Fields Generated by the filamentation (Weibel) Instability

Since magnetic fields are generated by the current structures produced in the filamentation (Weibel) instability (Dieckman et al. 2006), it is possible that "jitter" radiation (Medvedev 2000, 2006a,b; Fleishman 2006a,b; Medvedev et al. 2007; Workman et al. 2007; Fleishman & Toptygin 2007a,b) is an important emission process in GRBs. It should be noted that synchrotron- and 'jitter'-radiation are fundamentally the same physical processes (emission of accelerated charges in a magnetic field), but the relative importance of the two

regimes depends on the comparison of the deflection angle and the emission angle of the charges (Medvedev 2000). Emission via synchrotron- or "jitter"-radiation from relativistic shocks is determined by the magnetic field strength and structure and the electron energy distribution behind the shock, which can be computed self-consistently with RPIC simulations. The full RPIC simulations may actually help to determine whether the emission is more synchrotron-like or jitter-like.

The characteristic differences between Syncrotron- and jitter radiation are relevant for a more fundamental understanding the complex time evolution and/or spectral propertis of GRBs (prompt and afterglows) (Preece et al. 1998). For example, jitter radiation has been proposed as a solution of the puzzle that below their peak frequency GRB spectra are sometimes steeper than the "line of death" spectral index associated with synchrotron emission (Medvedev 2000, 2006a; Fleishman 2006a,b), i.e., the observed SED scales as $F_\nu \propto \nu^{2/3}$, whereas synchrotron SEDs should follow $F_\nu \propto \nu^{1/3}$, or even more shallow (e.g., Medvedev 2006a). Thus, it is crucial to calculate the emerging radiation by tracing electrons (positrons) in self-consistently evolved electromagnetic fields. This highly complex relativistic radiation-magneto-hydrodynamics-particle-acceleration problem requires sophisticated tools, such as multi-dimensional, relativistic, PIC methods.

3.3.   New Method of Calculating Synchrotron and Jitter Emission from Electron Trajectories in Self-consistently Generated Magnetic Fields

Consider a particle at position $\mathbf{r_0}(t)$ at time t (Fig. 3). At the same time, we observe the associated electric field from position $\mathbf{r}$. Because of the finite propagation velocity of light, we actually observe the particle at an earlier position $\mathbf{r_0}(t')$ along its trajectory, labeled with the retarded time $t' = t - \delta t' = t - \mathbf{R}(t')/c$. Here $\mathbf{R}(t') = |\mathbf{r} - \mathbf{r_0}(t')|$ is the distance from the charge (at the retarded time t') to the observer's position.
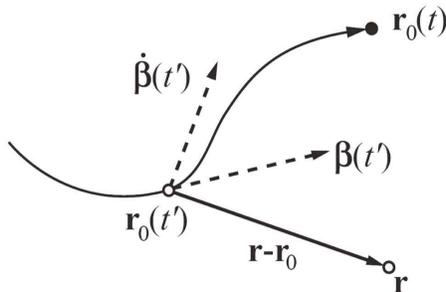

Fig. 3.— Definition of the retardation effect. From an observers point, r, one sees the particle at position $\mathbf{r_0}(t')$ where it was at retarded time t' (from Figure 2.2 in Hededal (2005)).

The retarded electric field from a charged particle moving with instantaneous velocity $\boldsymbol{\beta}$ under acceleration $\dot{\boldsymbol{\beta}}$ is expressed as (Jackson 1999),

$$\mathbf{E} \;\;=\;\; \frac{q}{4\pi\epsilon_0}\left[\frac{\mathbf{n}-\boldsymbol{\beta}}{\gamma^2(1-\mathbf{n}\cdot\boldsymbol{\beta})^3\mathrm{R}^2}\right]_{\mathrm{ret}} + \frac{q}{4\pi\epsilon_0 c}\left[\frac{\mathbf{n}\times\{(\mathbf{n}-\boldsymbol{\beta})\times\dot{\boldsymbol{\beta}}\}}{(1-\mathbf{n}\cdot\boldsymbol{\beta})^3\mathrm{R}}\right]_{\mathrm{ret}} \tag{1}$$

Here, $\mathbf{n}\equiv\mathbf{R}(\mathrm{t}')/|\mathbf{R}(\mathrm{t}')|$ is a unit vector that points from the particle's retarded position towards the observer. The first term on the right hand side, containing the velocity field, is the Coulomb field from a charge moving without influence from external forces. The second term is a correction term that arises when the charge is subject to acceleration. Since the velocity-dependent field falls off in distance as R^{-2}, while the acceleration-dependent field scales as R^{-1}, the latter becomes dominant when observing the charge at large distances $(R\gg 1)$.

The choice of unit vector $\mathbf{n}$ along the direction of propagation of the jet (hereafter taken to be the Z-axis) corresponds to head-on emission. For any other choice of $\mathbf{n}$ (e.g., $\theta=1/\gamma$), off-axis emission is seen by the observer. The observer's viewing angle is set by the choice of $\mathbf{n}$ $(n_{\mathrm{x}}^2+n_{\mathrm{y}}^2+n_{\mathrm{z}}^2=1)$. After some calculation and simplifying assumptions (for detailed derivation see Hededal 2005) the total energy W radiated per unit solid angle per unit frequency can be expressed as

$$\frac{d^2W}{d\Omega d\omega} \;\;=\;\; \frac{\mu_0 c q^2}{16\pi^3}\left|\int_{\infty}^{\infty}\frac{\mathbf{n}\times[(\mathbf{n}-\boldsymbol{\beta})\times\dot{\boldsymbol{\beta}}]}{(1-\boldsymbol{\beta}\cdot\mathbf{n})^2}e^{i\omega(t'-\mathbf{n}\cdot\mathbf{r_0}(\mathrm{t}')/c)}dt'\right|^2 \tag{2}$$

This equation contains the retarded electric field from a charged particle moving with instantaneous velocity $\boldsymbol{\beta}$ under acceleration $\dot{\boldsymbol{\beta}}$, and only the acceleration field is kept since the velocity field decreases rapidly as $1/R^2$. The distribution over frequencies of the emitted radiation depends on the particle energy, radius of curvature, and acceleration. These quantities are readily obtained from the trajectory of each charged particle.

Since the jet plasma has a large velocity Z-component in the simulation frame, the radiation from the particles (electrons and positrons) is heavily beamed along the Z-axis as jitter radiation (Medvedev 2000, 2006a; Medvedev et al. 2007; Workman et al. 2007; Fleishman & Toptygin 2007a,b).

4. Radiation from a gyrating electron

In the previous section we discussed how to obtain the retarded electric field from relativistically moving particles (electrons) observed at large distance. Using eq. 2 we calculated
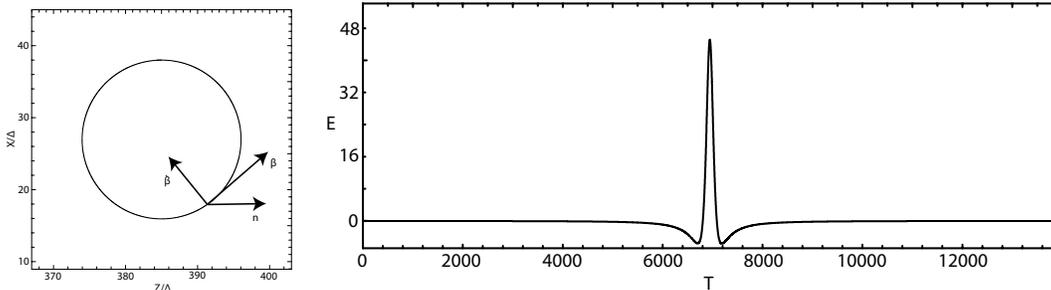
Fig. 4.— The path of a charged particle moving in a homogenous magnetic field (left panel) (with $\gamma = 15.8$). The particle produces a time-dependent, retarded electric field. An observer situated at a large distance along the **n**-vector sees the retarded electric field from the gyrating particle (right panel). As a result of relativistic beaming, the field is seen as pulses peaking when the particle moves directly towards the observer (Rybicki & Lightman 1979).
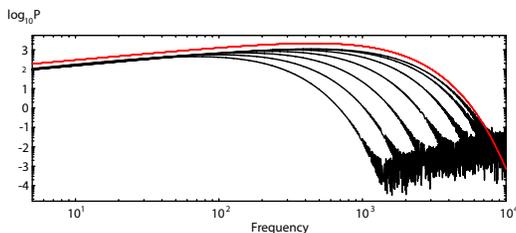

Fig. 5.— The observed power spectrum from a single charged particle, gyrating in a magnetic field at different viewing angles. The viewing angles are 0° (head-on), 1°, 2°, 3°, 4°, 5°, and 6° ($n_y \neq 0$) and the peak frequencies are 448, 408, 318, 222, 148, 98, and 85, respectively. At larger angles, frequencies above the Nyquist frequency are strongly damped. The units on both axes are arbitrary. The theoretical synchrotron spectrum for a viewing angle equal to 0° is plotted for comparison as a red curve (multiplied by 2 for clarity).

the time evolution of the retarded electric field and the spectrum from a gyrating electron in a uniform magnetic field to verify the technique used in this calculation. This calculation agrees with that done by Hededal (2005). Confirmation of those results is the first step towards validation of the implementation of the method in our code. In order to verify the basic properties of single particle emission (Jackson 1999), we have computed the spectrum for head-on and off angle observations for two Lorentz factors (15.8 and 40.8). The angles of off-angle observations are specified by n_y ($n_y^2 + n_z^2 = 1$). Here we kept the same gyroradius while increasing the magnetic field strength. The Nyquist frequency is defined as $\omega_N = 1/2\Delta t$ where Δt is the simulation time step. The frequencies are sampled in a logarithmic scale.
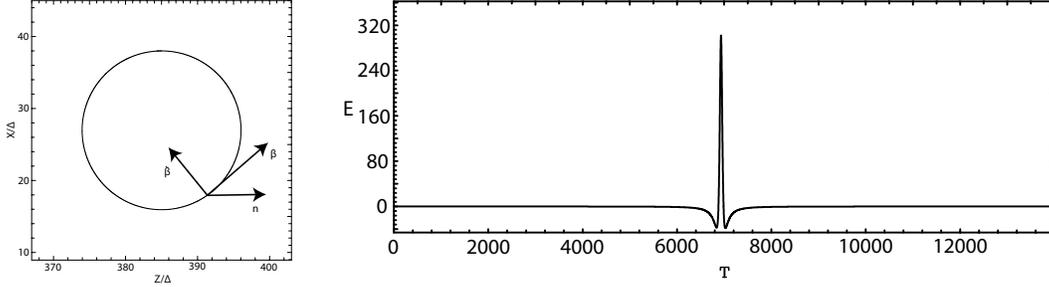
Fig. 6.— The path of a charged particle moving in a homogenous magnetic field (left panel) ($\gamma = 40.8$). The particle produces a time dependent electric field. An observer situated at great distance along the n-vector sees the retarded electric field from the gyrating particle (right panel). As a result of relativistic beaming, the field is seen as pulses peaking when the particle moves directly towards the observer.
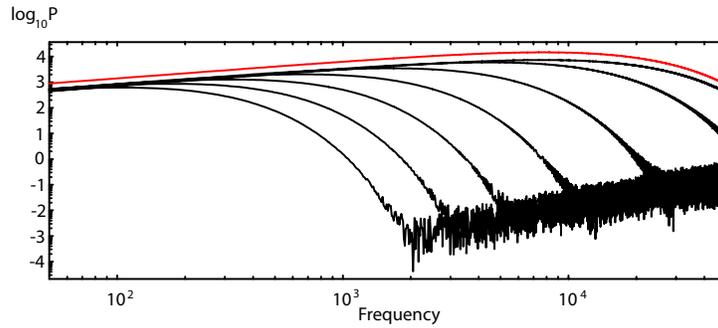

Fig. 7.— The observed power spectrum from a single charged particle, gyrating in a magnetic field at different viewing angles. The viewing angles are $0°$, $1°$, $2°$, $3°$, $4°$, $5°$, and $6°$ ($n_y \neq 0$) and their peak frequencies are 7642, 4395, 1648, 666, 316, 166, and 133, respectively. The critical frequency $f_c = \frac{3}{2}\gamma^3 \left(\frac{c}{\rho}\right) = 2309$, where $\rho = 11.03$. With larger angles the frequencies above the Nyquist frequency are strongly damped. The units on both axes are arbitrary. The theoretical synchrotron spectrum for a viewing angle equal to $0°$ is plotted for comparison as a red curve (multiplied by 2 for clarity).

First the case with the lower Lorentz factor ($\gamma = 15.8$) is calculated. The electron gyrates in the $x - z$-plane with the uniform magnetic filed (B_y) and the results are shown in Figures 4 & 5. The spectra observed far from the electron at angles with respect to the z direction are shown in Fig. 5. The critical frequency $f_c = \frac{3}{2}\gamma^3 \left(\frac{c}{\rho}\right) = 148$, where $\rho = 11.03$. The higher frequencies ($> f_c$) are strongly damped with increasing angles as $e^{(-f/f_c)}$, see Jackson (1999) and Melia (2001). We have very good agreement between the spectrum obtained from the simulation and the theoretical synchrotron spectrum expectation (red

curve) from eq. 3 (eq. 7.10 (Hededal 2005)).

Synchrotron radiation with the full angular dependency for the parallel direction is given by (Jackson 1999),

$$\frac{d^2W_{||}}{d\omega d\Omega} = \frac{\mu_0 cq^2\omega^2}{12\pi} \left(\frac{r_{\rm L}\theta_\beta^2\beta^2}{c}\right)^2 \frac{|K_{\frac{2}{3}}(\chi/\sqrt{\cos\theta\beta^3})|^2}{(\cos\theta\beta^3)^2},$$ (3)

where θ is the angle between $\mathbf{n}$ and the orbital plane $\theta_\beta^2 \equiv 2(1 - \beta\cos\theta)$, $\chi = \omega r_{\rm L}\theta_\beta^3/3c$ and $r_{\rm L}$ the gyro-radius $\gamma mv/(qB)$. For $\beta \to 1$ and $\theta \to 0$ this expression converges toward the solution one normally finds in text books (Jackson 1999; Rybicki & Lightman 1979; Melia 2001).

For a higher Lorentz factor ($\gamma = 40.8$) several differences are found. As expected, the peak value of the retarded electric field is much larger than that in the case of a lower Lorentz factor. The width of the spike is narrower, as shown in Fig. 6. The frequencies of the peak value are larger than those in the case of lower Lorentz factor, as shown in Fig. 7.

These results validate the technique used in our code. It should be noted that the method based on the integration of the retarded electric fields calculated by tracing many electrons described in the previous section can provide a proper spectrum in turbulent electromagnetic fields. On the other hand, if the formula for the frequency spectrum of radiation emitted by a relativistic charged particle in instantaneous circular motion is used (Jackson 1999; Rybicki & Lightman 1979), the complex particle accelerations and trajectories are not properly accounted for and the jitter radiation spectrum is not properly obtained (for details see Hededal 2005).

5. Discussion

The procedure used to calculate jitter radiation using the technique described in the previous section has been implemented in our code.

In order to obtain the spectrum of synchrotron (jitter) emission, we consider an ensemble of electrons randomly selected in the region where the filamentation (Weibel) instability has fully developed, and electrons are accelerated in the generated magnetic fields. We calculate emission from about 20,000 electrons during the sampling time, $t_{\rm s} = t_2 - t_1$ with Nyquist frequency $\omega_{\rm N} = 1/2\Delta t$ where Δt is the simulation time step and the frequency resolution $\Delta\omega = 1/t_{\rm s}$. However, since the emission coordinate frame for each particle is different, we accumulate radiation at fixed angles in simulation system coordinates after transforming from the individual particle emission coordinate frame. This provides an intensity spectrum

as a function of angle relative to the simulation frame Z-axis (this can be any angle by changing the unit vector $\mathbf{n}$ in eq. (1)). A hypothetical observer in the ambient medium (viewing the external GRB shock) views emission along the system Z-axis. This computation is carried out in the reference frame of the ambient medium in the numerical simulation. For an observer located outside the direction of bulk motion of the ambient medium, e.g., internal jet shocks in an ambient medium moving with respect to the observer, an additional Lorentz transformation would be needed along the line of sight to the observer. The spectra obtained from the simulations will be rescaled with a realistic time scale and relativistic Doppler shift. In electron-ion jets, the larger mass ratio (> 100) will provide enhanced electron acceleration compared to a mass ratio of 20 used here (Hededal 2005; Hededal & Nordlund 2005; Spitkovsky 2008).

Emission obtained by the method described above is self-consistent, and automatically accounts for magnetic field structures on the small scales responsible for jitter emission. By performing such calculations for simulations with different parameters, we can then investigate and compare the quite contrasted regimes of jitter- and synchrotron-type emission (Medvedev 2000) for prompt and afterglows. The feasibility of this approach has been demonstrated and implemented (Hededal & Nordlund 2005; Hededal 2005). Thus, we will be able to address the issue of low frequency GRB spectral index violation of the synchrotron line of death (Preece et al. 1998; Medvedev 2006a).

Since the emitted radiation is computed during the acceleration step in the code we can self-consistently include the effects of radiative losses (e.g., Noguchi, Liang, & Nishimura 2004). Radiative losses may not affect the global dynamics on our simulation timescales, but may be important for particles with the highest Lorentz factors.

REFERENCES

Achterberg, A., Gallant, Y. A., Kirk, J. G., & Guthmann, A. X. 2001, MNRAS, 328, 393

Bednarz, J., & Ostrowski, M. 1998, PRL, 80, 3911

Bednarek, W., Kirk, J.G., & Mastichiadis, A. 1996, A&A, 307, 17

Birdsall, C. K., & Langdon, A. B. 2005, Plasma Physics via Computer Simulation (6th ed.; IOP Publishing Ltd)

Blandford, R. & Eichler, D. 1987, Phys. Rep., 154, 1

Brainerd, J.J. 2000, ApJ, 536, 628

Buneman, O., 1993, *Tristan*, in Computer Space Plasma Physics: Simulation Techniques and Software, edited by H. Matsumoto Matsumoto & Y. Omura, p. 67, Terra Scientific Publishing Company, Tokyo

Chang, P., Spitkovsky, A., & Arons, J. 2008, ApJ, 674, 378 (arXiv:0704.3832)

Dawson, J. M. 1983, Rev. Mod. Phys., 55, 403

Dieckmann, M. E., Frederiksen, J. T., Bret, A., & Shukla, P.K. 2006, Phys. Plasmas, 13, 112110

Dieckmann, M. E., Shukla, P. K. & Drury, L. O. C. 2008, ApJ, in press

Eichler, D. and Waxman, E. 2005, ApJ, 627, 861

Ellison, D. C. 2001, Prog. Theor. Phys. Suppl., 143, 125

Ellison, D. C. & Double, G. P. 2002, Astroparticle Phys. 18, 213

Ellison, D. C., & Vladimirov, A. 2008, ApJ, 673L

Fermi, E. 1949, Phys. Rev. 75, 1169

Fleishman, G. D. 2006a, ApJ, 638, 348

Fleishman, G. D. 2006b, MNRAS, 365, L11

Fleishman, G. D. & Toptygin, I. N. 2007a, PRE, 76, 7401

Fleishman, G. D. & Toptygin, I. N. 2007b, MNRAS, 381, 1473

Frederiksen, J. T., Hededal, C. B., Haugbølle, T., & Nordlund, Å. 2003, Proc. From 1st NBSI on Beams and Jets in Gamma Ray Bursts, held at NBIfAFG/NORDITA, Copenhagen, Denmark, August, 2002, (arXiv:astro-ph/0303360)

Frederiksen, J. T., Hededal, C. B., Haugbølle, T., & Nordlund, Å. 2004, ApJ, 608, L13

Gallant, Y. A., 2002, Particle Acceleration at Relativistic Shocks, in Relativistic Flows in Astrophysics, eds. A. W. Guthmann, M. Georganopoulos, A. Marcowith, & K. Manolokou, Lecture Notes in Physics, Springer Verlag. (arXiv:astro-ph/0201243)

Gallant, Y. A. & Achterberg, A. 1999, MNRAS, 305, L6

Gruzinov, A. 2001, ApJ, 563, L15

Heavens, A. F. & Drury, L. O. 1988, MNRAS, 235, 997

Hededal, C.B., 2005, PhD thesis (arXiv:astro-ph/0506559)

Hededal, C. B. and Nishikawa, K.-I. 2005, ApJ, 623, L89

Hededal, C.B., & Nordlund, Å. 2005, submitted to ApJL (arXiv:astro-ph/0511662)

Hededal, C. B., Haugbølle, T., Frederiksen, J. T., and Nordlund, Å. 2004, ApJ, 617, L107

Hickory & Eastwood, J. W., 1988, Computer Simulation using Particles, McGraw-Hill, second edition

Hoshino, M., 2008, ApJ, 672, 940

Jackson, J. D. 1999, *Classical Electrodynamics*, Interscience

Jaroschek, C. H., Lesch, H., & Treumann, R. A. 2005, ApJ, 618, 822

Kirk, J. G. & Schneider, P. 1987, ApJ, 315, 425

Kirk, J. G., Guthmann, A. W., Gallant, Y. A., and Achterberg, A. 2000, ApJ, 542, 235

Kobayashi, S., Zhang, B., Meszaros, P. & Burrows, D. D. 2007, ApJ, 655, 391

Lemoine, M. & and G. Pelletier, G. 2003, ApJ. 589, L73

Lyutikov, M. 2006, New Journal of Physics, 8, 119

Medvedev, M. V. 2006a, ApJ, 637, 869

Medvedev, M. V. 2006b, ApJ, 651, L9

Medvedev, M. V. 2000, ApJ, 540, 704

Medvedev, M.V. & Loeb, A. 1999, ApJ, 526, 697

Medvedev, M.V. & Spitkovsky, A. 2007, in preparation

Medvedev, M. V., Silva, L. O. & Kamionkowski, M. 2006, ApJ, 642, L1

Medvedev, M. V., Fiore, M., Fonseca, R. A., Silva, L. O., and Mori, W. B. 2005, ApJ, 618, L75

Medvedev, M. V., Lazzati, D., Morsony, B. J., & Workman, J. C. 2007, ApJ, 666, 339

Melia, F. 2001, *Electrodynamics*, The University of Chicago Press

Meszaros, P. 2002, ARAA 40, 137

Meszaros, P. 2006, Rept. Prog. Phys. 69, 2259

Meszaros, P., Ramirez-Ruiz, E., & Rees, M. J. 2001, ApJ, 554, 660

Meszaros, P., Rees, M. J., Wijers, R. A. M. J. 1998, ApJ, 499, 301

Milosavljevic, M., & Nakar, E. 2006a, ApJ, 641, 978

Milosavljevic, M., & Nakar, E. 2006b, ApJ, 651, 979

Milosavljevic, M., Nakar, E., & Spitkovsky, A. 2006, ApJ, 637, 765

Nakar, E. 2007, Phys. Reports, 442, 166 (arXiv:astro-ph/0703129)

Niemiec, J., & Ostrowski, M. 2004, ApJ, 610, 851

Niemiec, J., & Ostrowski, M. 2006, ApJ, 641, 984

Niemiec, J., Ostrowski, M., & Pohl, M. 2006, ApJ, 641, 984

Niemiec, J., Pohl, M., Stroman, T. & Nishikawa, K.-I. 2008, ApJ, submitted, (arXiv:astro-ph/0802.2185)

Nishikawa, K.-I., Hardee, P., Richardson, G., Preece, R., Sol, H., & Fishman, G.J. 2003, ApJ, 595, 555

Nishikawa, K.-I., Hardee, P., Richardson, G., Preece, R., Sol, H., & Fishman, G.J. 2005a, ApJ, 622, 927

Nishikawa, K.-I., Hardee, P., Hededal, C. B., Richardson, G., Preece, R., Sol, H., & Fishman, G.J. 2005b, High Energy Gamma-Ray Astronomy, AIP Conf. Proc. vol 745, p.534 (arXiv:astro-ph/0410193)

Nishikawa, K.-I., Hardee, P., Hededal, C. B., & Fishman, G.J. 2006a, ApJ, 642, 1267

Nishikawa, K.-I., Hededal, C. B., Hardee, P., Kouveliotou, C., Fishman, G. J., & Mizuno, Y., 2006b, Astrophys. & Space Science, DOI 10.1007/s10509-006-9234-5

Nishikawa, K.-I., Mizuno, Y., Fishman, G. J., & Hardee, P., 2008, contributed talk at the workshop: High Energy Phenomena in Relativistic Outflows (HEPRO), Dublin, 24-28 September 2007 (arXiv:0801.4390)

Noguchi, K., Liang, E., & Nishimura, K. 2004, submitted to Phys. Plasmas, (arXiv:astro-ph/0412310)

Ostrowski, M. & Bednarz, J. 2002, A&A, 394, 1141

Panaitescu, A., Kumar, P., 2001, ApJ, 560, L49

Piran, T. 1999, Phys. Rep., 316, 575

Piran, T. 2000, Phys. Rep., 529, 333

Piran, T. 2005a, Rev. Mod. Phys. 76, 1143

Piran, T. 2005b, in the proceedings of Magnetic Fields in the Universe, Angra dos Reis, Brazil, Nov. 29-Dec 3, 2004, Ed. E. de Gouveia del Pino, (arXiV:astro-ph/0503060)

Preece, R. D.,, Briggs, M. S., Mallozzi, R. S., Pendleton, G. N., Paciesas, W. S., & Band, D. L. 1998, ApJ, 506, L23

Pruet, J., Abazajian, K., Fuller, G. M. 2001, Phys. Rev. D. 64, 063002-1

Ramirez-Ruiz, E., Nishikawa, K.-I., & Hededal, C. B., 2007, ApJ, 671, 1877

Rybicki, G. B., & Lightman, A. P. 1979, *Radiative Processes in Astrophysics*, John Wiley & Sons, New York

Sari, R., Piran, T., & Naryan, R. 1998, ApJ, 497, L17

Silva, L. O., Fonseca, R. A., Tonge, J,.W., Dawson, J. M., Mori, W.B., & Medvedev, M. V., 2003, ApJ, 596, L121

Spitkovsky, A. 2005, in Proceeding of Astrophysical Sources of High Energy Particles and Radiation, eds. T. Bulik, B. Rudak, G. Madejski, AIP Conf. Proc., v. 801, pp. 345-350 (arXiV:astro-ph/0603211)

Spitkovsky, A. 2008, ApJ, 673L

Vieti, M. 2003, ApJ, 591, 954

Vladimirov, A., Ellison, D. C., Bykov, A. 2006, ApJ, 652, 1246

Waxman, E. 2006, Plasma Phys. Control. Fusion, 48 B137 (arXiv:astro-ph/0607353)

Waxman, E. 2003, Lect. Note Phys. 598, 393 (arXiV:astro-ph/0303517)

Weibel, E. S. 1959, Phys. Rev. Lett., 2, 83

Workman1, J. C., Morsony1, B. J., Lazzati1, D. & Medvedev, M. V. 2007, MNRAS, submitted (arXiv:astro-ph/0703420)

Yost, S. A.; Harrison, F. A.; Sari, R.; Frail, D. A. 2003, ApJ, 597, 459

Zhang, B. 2007, Chin. J. Astron. Astrophys. 7, 1 (arXiv:astro-ph/0701520)

Zhang, B. & Meszaros, P. 2004, Int. J. Mod. Phys., A19, 2385 (arXiV:astro-ph/0311321)